Theoretical Photoabsorption Spectra of ClOOCl and Cl$_2$O

A. Toniolo,[†] M. Persico,* and D. Pitea[†]

Dipartimento di Chimica Fisica ed Elettrochimica, Università di Milano, via Golgi 19, I-20133 Milano, Italy, and Dipartimento di Chimica e Chimica Industriale, Università di Pisa, via Risorgimento 35, I-56126 Pisa, Italy

Received: March 27, 2000; In Final Form: May 25, 2000

We calculated transition energies and oscillator strengths of ClOOCl and Cl$_2$O in the Franck−Condon region with ab initio techniques. We describe 8 singlet excited states for ClOOCl and 13 excited states for Cl$_2$O. The photoabsorption spectra are simulated by a semiclassical approach, which takes into account the vibrational phase space distribution in the ground state and the geometry dependence of excitation energies and transition dipoles. We present an unambiguous assignation of the available UV spectra, which is preliminary to the interpretation of the photochemistry of these compounds.

1. Introduction

In the last fifteen years, the photochemistry of chlorine oxides has received considerable attention: the importance of the ozone loss catalytic cycles has made advisable to understand the photodissociation reactions of the chlorine−oxygen containing molecules present in the stratosphere.[1−3]

Among the important chlorine−oxygen compounds, the spectroscopy of ClO has been investigated theoretically by us and others,[4−6] and rather complete potential energy surfaces for ClO$_2$ have been presented.[7] ClOOCl and Cl$_2$O have been paid less attention by computational chemists.
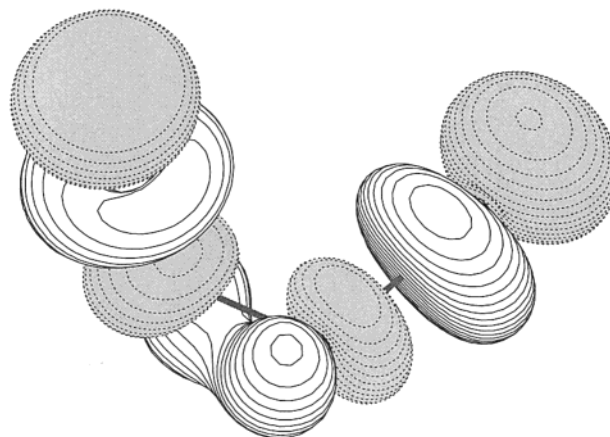
It is now accepted that the most important catalytic cycle that results in ozone depletion in the Antarctic stratosphere starts with the self-reaction of ClO radicals and involves the formation of a chlorine peroxide ClOOCl molecule.[8] The absorption of radiation breaks preferably one of the two Cl−O bonds:[3,9−11]

$$ClOOCl \xrightarrow{h\nu} ClOO + Cl \rightarrow 2Cl + O_2$$

while the alternative dissociation

$$ClOOCl \xrightarrow{h\nu} 2ClO$$
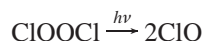
proceeds with low (≈ 0.1)[11] or vanishing[10] quantum yields. Stanton and Bartlett,[12] in an ab initio theoretical investigation in 1993, rationalized the preference for Cl−O bond cleavage: in a molecular orbital picture, the six lowest excited states involve promotion of a valence electron in a σ^*_{Cl-O} orbital. To understand the photochemistry of ClOOCl, we simulate the structure of the UV spectrum; in fact, the band assignment and the rationalization of the electronic configuration of the excited states is basic to obtaining a clearer picture of the mechanisms of the photodissociations. The experimental electronic spectrum of the ClO dimer[2,9,13−16] shows a relatively strong and broad absorption feature with a maximum at 245 nm (5.06 eV) and a tail which extends to wavelengths above 360 nm (3.4 eV). The weak cross sections in the long-wavelength tail are difficult to

* To whom correspondence should be addressed at the Università di Pisa.
† Università di Milano.

Figure 1. LUMO natural orbital of the ClOOCl molecule for the 3^{1}B state, labeled as σ^*_a.
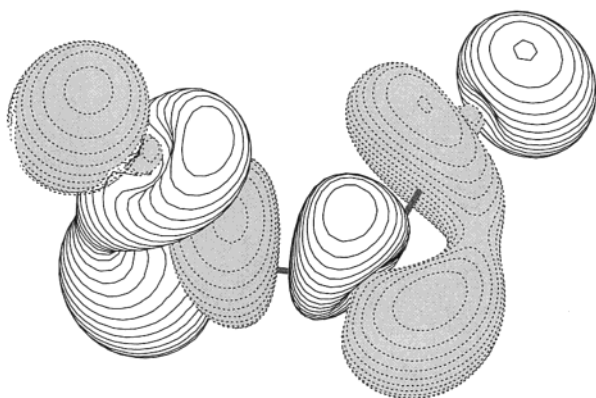
measure and are preferably evaluated by extrapolation from shorter wavelengths;[2] yet, this absorption is important because it permits the photodissociation in the near-UV.

Dichlorine monoxide, Cl$_2$O, is thought to play a minor role in the stratospheric chemistry. However, this is the acid anhydride of hypochlorous acid, HOCl, one of the most important chlorine reservoir compounds in the atmosphere. Cl$_2$O reacts with water on the surface of polar stratospheric clouds in an equilibrium reaction to produce HOCl.[17,18] Consequently, the photochemistry of Cl$_2$O has received attention in recent years.[19−21] Irradiation below 300 nm leads primarily to formation of ClO + Cl, with minor channels leading to O(^{3}P) or O(^{1}D) and molecular chlorine or two chlorine atoms. The absorption spectrum[22,23] contains overlapping continuous bands in the 620−500, 500−380, 380−220, 180−150, and 145−130 nm photon energy regions (see Figure 4). The attribution of these bands and the characterization of the electronic excited states are preliminary to the understanding of the photochemistry of Cl$_2$O.

We calculated electronic energies and transition dipole moments for ClOOCl and Cl$_2$O in the Franck−Condon region; in section 2, we give the details of the methods employed. We also obtained the frequency-dependent absorption cross sections with the semiclassical technique described in section 3. In section 4, we report the simulation of the photoabsorption

ClOOCl and Cl$_2$O Photoabsorption Spectra

J. Phys. Chem. A, Vol. 104, No. 31, 2000 **7279**

Figure 2. LUMO + 1 natural orbital of the ClOOCl molecule for the 3^1B state, labeled as σ_b^*.
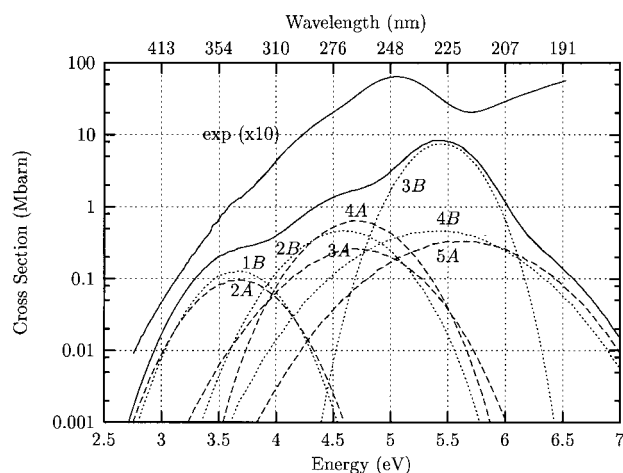
Figure 3. Simulated UV spectrum of the ClOOCl molecule. The recommended experimental cross section (ref 2) is also shown; for the sake of clarity, it is displaced upward by 1 unit in the log scale. Dashed lines, partial calculated cross sections; full line, total cross sections.
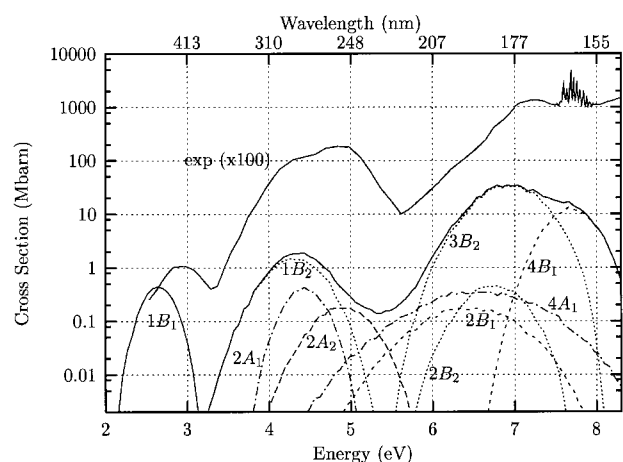
Figure 4. Simulated UV spectrum of the Cl$_2$O molecule. The experimental cross section is also shown; for the sake of clarity, it is displaced upward by 2 units in the log scale. $\lambda > 200$ nm is from Knauth et al.;[22] $\lambda < 200$ nm is from Motte-Tollet et al.[23] Dashed lines, partial calculated cross sections; full line, total cross sections.

spectra and the analysis of the electronic structure of the two molecules. The main conclusions are summarized in section 5.

2. Computational Methods

The study of the absorption spectra of ClOOCl and Cl$_2$O is part of a wider theoretical study of the photochemistry of both molecules carried out in our laboratory. The computational methods used and the atomic bases employed have been chosen according to preliminary calculations. The techniques used for the two molecules, described separately in the following discussion, have been chosen in order to reproduce correctly dissociations and other geometrical rearrangements.

2.1. Chlorine Peroxide, ClOOCl. We determined electronic energies and wave functions by the Complete Active Space Configuration Interaction (CAS-CI), using the GAMESS program.[24]

The molecular orbitals involved in the CI expansion were chosen in order to contain all valence orbitals of the separated atoms: the 2s and the three 2p orbitals for the oxygen atoms and the 3s and the three 3p orbitals for the chlorine atoms. Therefore, we used CAS-CI wave functions with 26 electrons in 16 orbitals. The numbers of determinants generated was 313 600; at the C_2 geometries, the configurations were equally distributed in the A and B irreps. The molecular orbitals for the CI were provided by formally closed-shell SCF calculations, with floating occupation numbers.[4] In this scheme, the populations of the MOs are distributed along the energy axis according to Gaussian functions centered at the MO energies. In this work, we adopted a Gaussian width of 0.35 hartree. This procedure guarantees a partial occupation and optimization of the low-lying virtual orbitals and, consequently, a faster convergence of the CI expansion and a better description of the electronic states. We adopted Ahlrichs's VTZ basis set[25] and supplemented it with polarization d functions of Dunning's cc-pVTZ basis set[26,27] on chlorine and oxygen atoms. With this procedure, we calculated nine singlet electronic states: five A states and four B states.

The equilibrium geometry of the ground state was obtained with two different methods; the first one has already been indicated as CAS-CI. The second one was a CASSCF wave function with 10 electrons in 10 orbitals, obtained with the MOLCAS program;[28] in the latter case, we were able to calculate normal coordinates and vibrational frequencies.

2.2. Dichlorine Monoxide Cl$_2$O. This molecule belongs to the C_{2v} symmetry group at the equilibrium geometry but we also explored configurations belonging to the C_s symmetry group. We determined wave functions and electronic energies by Multi Reference second-order perturbation Configuration Interaction, with programs developed in our laboratory. The configurational spaces were selected as follows: the first space was a CAS with 14 electrons in 9 orbitals and all single and double excitations from this space to the next three virtual orbitals, limiting the maximum excitation level to four, whereas the second space was a CAS with 20 electrons in 12 orbitals. The two spaces were merged to yield 27 665 A' determinants (13 871 A_1 and 13 794 B_2 at C_{2v} geometries) and 27 490 A'' (13 750 A_2 and 13 740 B_1 at C_{2v} geometries). The variational wave functions were the basis for a diagrammatic[29,30] quasi-degenerate perturbation theory treatment,[31] with a Møller–Plesset partition of the Hamiltonian. Again, we used MOs with floating occupation numbers,[4] as described briefly in the previous subsection. As a basis set, we adopted Dunning's cc-pVTZ[26,27] and supplemented it with diffuse s and p functions[32] on the oxygen atom for a better description of the excited states. The s diffuse exponents were 0.0608 and 0.024, and the p ones were 0.0532 and 0.021.

The equilibrium geometry and the normal modes were found by fitting the calculated energies at selected geometries with a quadratic function of the internal coordinates.

3. Semiclassical Calculation of Integral Cross Sections

We calculated frequency-dependent oscillator strengths for each excited state with a semiclassical approach similar to that of ref 33, which takes into account the vibrational mode amplitudes in the ground state and the variation of transition energies and dipoles as functions of the nuclear geometry. The oscillator strength density is given by

$$\frac{df}{d\nu} = \frac{2}{3}h\nu \int d\tau W(\tau)|\mu_{gr,ex}(\tau)|^2 \delta\left[\nu - \frac{E_{ex} - E_{gr}}{h}\right] \quad (1)$$

If $df/d\nu$ is expressed in atomic units, the differential cross section σ in Mbarn is given by $\sigma(\nu) = 4.03(df/d\nu)$. Here, $\tau = \tau(\mathbf{R}, \mathbf{P})$ represents an initial point in the phase space and $d\tau$ is the corresponding volume element. The delta function selects only those phase space points that meet the resonance condition $E_{ex} - E_{gr} = h\nu$; here, E_{gr} is the ground-state energy, calculated as the energy at the equilibrium geometry plus the zero-point energy, E_{ex} is the kinetic plus excited-state potential energy, and $\mu_{gr,ex}$ is the transition dipole. The function $W_{gr}(\tau)$ weights each initial point τ according to the ground-state probability distribution. W_{gr} has been chosen as the Wigner distribution function for the ground vibrational level:

$$W_{gr}(\mathbf{R}, \mathbf{P}) = \prod_i \exp[-\omega_i \mathbf{R_i}^2]\exp\left[-\frac{1}{4}\omega_i \mathbf{P_i}^2\right] \quad (2)$$

In this expression, the product runs over all the normal coordinates: R_i represents the displacement along the i-th normal coordinate of ω_i frequency and P_i its associated momentum.

After integration with respect to the frequency, ν, of eq 1, we obtain the total oscillator strength for a given transition in a frequency range ν' to ν'':

$$f_{\nu',\nu''} = \frac{2}{3}\int_{V(\nu',\nu'')}d\tau W_{gr}(\tau)|\mu_{gr,ex}(\tau)|^2[E_{ex}(\tau) - E_{gr}] \quad (3)$$

In practice, the integral is done by Monte Carlo sampling of the points in the phase space: for each, the energy difference $E_{ex}(\tau) - E_{gr}$ determines to which box $[\nu',\nu'']$ of a frequency histogram the contribution is added.

The total electronic spectrum is obtained as the superposition of the bands computed in this way for all the excited states. To do this, one needs an analytical expression of the potential energy surface and transition dipole in the Franck–Condon region for each excited state. Therefore, we fitted potential surfaces and transition dipoles with a linear function of the internal coordinates.

It is clear that the semiclassical approach outlined here is suitable for dissociative or weakly bound excited-state potential energy surfaces that give rise to continuous bands: it cannot reproduce in detail the vibrational structure associated with bound–bound transitions.

4. Results and Discussion

4.1. Chlorine Peroxide, ClOOCl. Recalling that the ClOOCl molecule belongs to the C_2 symmetry group at the equilibrium nuclear displacement, the electronic configuration can be written as

$$[core]....(13a)^2(12b)^2$$

Results of geometry optimizations in comparison with the experimental geometry are reported in Table 1. Both compu-

TABLE 1: Computed and Experimental Equilibrium Geometries[35] and Vibrational Frequencies[34] in cm^{-1} for the ClOOCl Molecule

	CAS-CI	CASSCF	exp
O–O (bohr)	2.7485	2.6170	2.6947
O–Cl (bohr)	3.3711	3.4053	3.2201
∠Cl–O–O (deg)	109.7	109.6	110.1
∠ClOOCl (deg)	83.2	86.8	81.9
τ		121	127
δ_{ClOO}		277	–
δ_{ClOO}		391	418
ν_{OCl}		526	543
ν_{OCl}		585	647
ν_{OO}		813	754

TABLE 2: Computed Transition Energies (ΔE) and Oscillator Strengths (f) of ClOOCl with the CAS-CI Method at the Experimental Equilibrium Geometry, Compared with Those Produced by Stanton and Bartlett with the EOM-CCSD Method and POL Basis Set[12]

	this work		Stanton and Bartlett	
	ΔE (eV)	f	ΔE (eV)	f
2^1A	3.52	3.1(−4)	3.91	1.9(−4)
3^1A	4.38	1.0(−3)	5.03	6.5(−4)
4^1A	4.50	2.1(−3)	5.41	1.4(−2)
5^1A	5.42	2.3(−3)	6.55	3.6(−3)
1^1B	3.48	4.7(−4)	3.88	2.1(−4)
2^1B	4.36	1.2(−3)	5.03	1.0(−2)
3^1B	4.93	3.3(−2)	5.42	7.9(−2)
4^1B	5.39	6.4(−4)	6.54	1.4(−3)

tational methods are demonstrated to be appropriate to describe the equilibrium configuration. Normal-mode analysis was performed only with CASSCF; Table 1 also shows the computed and experimental vibrational frequencies.

With the CAS-CI method, we calculated eight electronic excited states: four A and four B states. Table 2 contains the transition energies and the oscillator strengths of each state at the experimental equilibrium geometry[35] of the ground-state. We also report the same quantities obtained by Stanton and Bartlett.[12] We note considerable differences in transition energies from those of Stanton and Bartlett, from 0.4 eV for low-lying states to more than 1.1 eV for upper states. Even oscillator strengths appear to be quite different: in Stanton and Bartlett's calculations there were al least three states that gave rise to intense transitions, 4^1A, 2^1B, and 3^1B, whereas our results show that only one excited state is responsible for intense radiation absorption, the $3\ ^1B$. The role of the other states will be clearer in the spectrum simulation. It is interesting at this point to analyze the electronic configuration of the excited states: we calculated natural orbitals and occupations for each state and repeated the CI calculation, adopting for each state its natural orbitals as molecular basis. The results are summarized in Table 3; we reported symmetry, type, and occupation number of the HOMO, HOMO-1, LUMO, and LUMO + 1 natural orbitals for each state and the square coefficients of the most important electronic configurations. One could be surprised that every state is represented mainly by two mixed single excitations: in the natural orbital basis, they are the HOMO → LUMO and the HOMO-1 → LUMO + 1 transitions, $(a \to a)$ and $(b \to b)$ for the A states and $(a \to b)$ and $(b \to a)$ for the B states. This can be understood by considering the nature of the orbitals involved in the transitions and indicated in the table under the label "type". Every molecular orbital can be interpreted as the combination of two orbitals localized on the ClO moieties. With $n_\perp$, we indicate a nonbonding orbital perpendicular to the plane identified by the Cl and O atoms to which it belongs and the other O atom. The nonbonding orbitals, composed of atomic

ClOOCl and Cl$_2$O Photoabsorption Spectra

J. Phys. Chem. A, Vol. 104, No. 31, 2000 **7281**

TABLE 3: Electronic Configurations of the Excited States of ClOOCl: Symmetry, Type, and Occupation Numbers of Natural Orbitals of each A Excited State[a]

state		HOMO-1	HOMO	LUMO	LUMO + 1	$C^2_{H\rightarrow L}$	$C^2_{H-1\rightarrow L+1}$
2^{1}A	symm.	a	b	b	a	0.50	0.32
	type	$n_\perp$	$n_\perp$	σ^*_b	σ^*_a		
	occ.n.	1.6	1.4	0.7	0.5		
3^{1}A	symm.	b	a	a	b	0.48	0.32
	type	$n_\parallel$	$n_\parallel$	σ^*_a	σ^*_b		
	occ.n.	1.6	1.4	0.7	0.5		
4^{1}A	symm.	b	a	a	b	0.20	0.16
	type	$n_\parallel$	$n_\parallel$	σ^*_a	σ^*_b		
	occ.n.	1.5	1.4	0.7	0.5		
5^{1}A	symm.	b	a	a	b	0.34	0.32
	type	π_{ClO}	π_{ClO}	σ^*_a	σ^*_b		
	occ.n.	1.6	1.6	0.7	0.6		
1^{1}B	symm.	b	a	b	a	0.52	0.31
	type	$n_\perp$	$n_\perp$	σ^*_b	σ^*_a		
	occ.n.	1.6	1.4	0.7	0.5		
2^{1}B	symm.	b	a	b	a	0.53	0.29
	type	$n_\parallel$	$n_\parallel$	σ^*_b	σ^*_a		
	occ.n.	1.6	1.4	0.7	0.5		
3^{1}B	symm.	b	a	b	a	0.37	0.36
	type	$n_\perp$	$n_\perp$	σ^*_b	σ^*_a		
	occ.n.	1.5	1.5	0.6	0.6		
4^{1}B	symm.	a	b	b	a		
	type	π_{ClO}	π_{ClO}	σ^*_b	σ^*_a		
	occ.n.	1.6	1.6	0.7	0.6		

^{a} $C^2_{H\rightarrow L}$ and $C^2_{H-1\rightarrow L+1}$ represent the square of the CI coefficients of the singly excited configurations HOMO → LUMO and HOMO−1 → LUMO + 1, respectively.

orbitals lying in the same ClOO plane, are labeled as $n_\parallel$. With π_{ClO}, we indicate bonding orbitals obtained from two π orbitals for each ClO moiety. The label σ^* refers to antibonding orbitals; we emphasize that σ^*_a indicates an orbital with antibonding character solely along the ClO axis whereas, for symmetry reasons, σ^*_b denotes an orbital with antibonding character both along the ClO and along the OO axis. In Figures 1 and 2, we report the LUMO (σ^*_a) and LUMO+1 (σ^*_b) orbitals for the 3^{1}B state that carries the largest oscillator strength. Therefore, we emphasize that every excited state is of an antibonding nature, mainly along the Cl−O bond, but also partially along the O−O bond. This observation does not agree with the results of Stanton and Bartlett,[12] which attributed an exclusive σ^*_{Cl-O} character to every calculated excited state. On the contrary, we believe that the partial σ^*_{O-O} nature of excited states can help to interpret the evidence for the nonnegligible photodissociation of ClOOCl in two ClO fragments.[11]

At this point, we try to answer the obvious question: why is every excited state expressed as a mixing of two single excitations? Let us consider two nonbonding orbitals n_1, n_2 and two antibonding orbitals σ^*_1, σ^*_2 localized in the two ClO moieties. Two $n \rightarrow \sigma^*$ configurations have A symmetry:

$$(n_1 + n_2)(\sigma^*_1 + \sigma^*_2) = n_1\sigma^*_1 + n_2\sigma^*_2 + n_2\sigma^*_1 + n_1\sigma^*_2$$
$$(n_1 - n_2)(\sigma^*_1 - \sigma^*_2) = n_1\sigma^*_1 + n_2\sigma^*_2 - n_2\sigma^*_1 - n_1\sigma^*_2$$

The two first terms in both rhs represent transitions localized in each moiety, and the two others represent zwitterionic states; therefore, combining these two configurations with equal coefficients, we delete the zwitterionic components from the wave function. The same is true for the B symmetry.

TABLE 4: Computed and Experimental Equilibrium Geometries[36] and Vibrational Frequencies[37] in cm^{-1} of the Cl$_2$O Molecule

	this work	exp
O−Cl (bohr)	3.2388	3.0247
∠Cl−O−O (deg)	113.95	110.89
δ_{ClOCl}	227	296
ν_{OCl}	543	639
ν_{OCl}	632	686

The spectral simulation was done by sampling 50 million points in the phase space. Temperature effects were not taken into account, as our phase space distribution corresponds to the vibrational ground state. As the torsional mode in ClOOCl has a low frequency (theoretical and experimental values: 121 and 127 cm^{-1}), one may expect significant populations of the vibrationally excited states. However, the potential energy curves of the excited electronic states are rather flat around the equilibrium dihedral angle for the ground state, so the dependence of the simulated spectra on the distribution of torsional angles should not be important.

In Figure 3, we report the bands due to each transition and the total absorption cross section. The maximum is at 227 nm (5.45 eV), with a cross section $\sigma = 8.4$ Mbarn. Experimentally, the maximum σ is 6.5 ± 0.6 Mbarn at 245 nm (5.06 eV).[2] As revealed in advance by the oscillator strengths calculated at the equilibrium geometry, the UV spectrum is dominated by the 1^{1}A → 3^{1}B transition, which gives rise to a broad band between 253 and 205 nm (4.9 − 6.0 eV). Also, according to Stanton and Bartlett this is the most important transition, but they calculate it about 0.5 eV higher and 2.4 times more intense. There are two more bands, due to the 4^{1}B and 5^{1}A states, superimposed in the same spectral region; together, they contribute about 9% of the maximum absorption. At longer wavelengths three more states appear to be responsible for nonnegligible absorption: 4^{1}A, 3^{1}A, and 2^{1}B. Their maximum is placed around 264 nm (4.7 eV), but they dominate the absorption up to 326 nm (3.8 eV), where it is fifty times lower than the maximum. In the simulated spectrum as well as in the experimental one, these absorptions produce a weak shoulder around 280 nm. The states 2^{1}A and 1^{1}B produce two superimposed small bands at about 340 nm (3.65 eV) with oscillator strength density about 80 times less intense than the maximum. The tail observed in the experimental spectrum is due to these states.

4.2. Dichlorine monoxide, Cl$_2$O. The equilibrium geometry of the Cl$_2$O molecule belongs to the C_{2v} symmetry group; the ground-state electronic configuration is

$$[core]....(2a_2)^2(9a_1)^2(7b_2)^2(3b_1)^2$$

The equilibrium displacement was derived by fitting the computed energies with a quadratic function. The geometry and the normal-mode analysis are reported in Table 4.

To reproduce the UV spectrum up to 8 eV,[23] we calculated 14 electronic states: four ^{1}A$_1$, three ^{1}A$_2$, four ^{1}B$_1$, and three ^{1}B$_2$. We show transition energies and oscillator strengths calculated at the equilibrium geometry in Table 5. We also show the results of similar calculations done recently by Del Bene et al.[38] and Nickolaisen et al.[20] on 5 and 7 excited singlets, respectively. We note that our results are similar to those produced by Del Bene having an average difference of 0.15 eV in vertical transition energies. In contrast, the excitation energies obtained by Nickolaisen are higher by 0.5 to 1 eV. This fact implies differences in the attribution of the UV spectral

TABLE 5: Computed Transition Energies and Oscillator Strengths of the Cl_2O Molecule, using the Perturbed MRCI Method, at the Equilibrium Geometry and, for comparison, Those Produced by Del Bene et al. with the EOM-CCSD(T) Method and the POL Basis Set[38] and by Nickolaisen et al. with the MRCISD Method and the cc-pVTZ Basis Set[20]

	this work		Del Bene et al.		Nickolaisen et al.	
	ΔE (eV)	f	ΔE (eV)	f	ΔE (eV)	f
2^1A_1	4.47	5.9(−4)	4.66	1.8(−3)	5.45	8.5(−5)
3^1A_1	5.35	1.2(−5)	−	−	−	−
4^1A_1	6.42	1.7(−3)	−	−	−	−
1^1A_2	4.39	0.0	4.23	0.0	4.97	0.0
2^1A_2	4.88	0.0	5.01	0.0	5.88	0.0
3^1A_2	6.44	0.0	−	−	−	−
1^1B_1	2.68	1.1(−3)	2.82	8.(−5)	3.42	1.4(−4)
2^1B_1	6.41	6.3(−4)	−	−	7.34	5.3(−3)
3^1B_1	6.58	1.3(−1)	−	−	−	−
4^1B_1	7.70	2.4(−3)	−	−	−	−
1^1B_2	4.39	1.1(−1)	4.23	1.0(−2)	4.98	7.7(−3)
2^1B_2	6.77	9.0(−3)	−	−	7.98	6.0(−6)
3^1B_2	7.04	7.2(−2)	−	−		

TABLE 6: Electronic Configurations of Excited States of the Cl_2O Molecule

state	electr. configuration
2^1A_1	$\sigma \rightarrow \sigma^*_{a_1}$
3^1A_1	$\pi^*\pi^* \rightarrow \sigma^*_{a_1}\sigma^*_{a_1}$
4^1A_1	$n \rightarrow \sigma^*_{b_2}$
1^1A_2	$\pi_{nb} \rightarrow \sigma^*_{a_1} + \pi^* \rightarrow \sigma^*_{b_2}$
2^1A_2	$\pi_{nb} \rightarrow \sigma^*_{a_1} - \pi^* \rightarrow \sigma^*_{b_2}$
3^1A_2	$n\, \pi^* \rightarrow \sigma^*_{a_1}\sigma^*_{a_1}$
1^1B_1	$\pi^* \rightarrow \sigma^*_{a_1}$
2^1B_1	$\pi \rightarrow \sigma^*_{a_1} + \pi_{nb} \rightarrow \sigma^*_{b_2}$
3^1B_1	$\pi_{nb} \rightarrow \sigma^*_{b_2} + \sigma\pi \rightarrow \sigma^*_{a_1}\sigma^*_{a_1}$
4^1B_1	$\pi^* \rightarrow Ryd(s)$
1^1B_2	$n \rightarrow \sigma^*_{a_1}$
2^1B_2	$\pi_{nb}\, \pi^* \rightarrow \sigma^*_{a_1}\sigma^*_{b_2}$
3^1B_2	$\sigma \rightarrow \sigma^*_{b_2}$

bands of the Cl_2O; as an example, they attribute the weak absorption peak at 427 nm (2.9 eV) to a spin-forbidden transition to the lowest-lying triplet state 1^3B_1, whereas we find at this energy the 1^1B_1 state. The calculations of oscillator strengths give very different results in the three works, which is understandable in view of the weakness of all transitions. In the following discussion, we shall try to reinterpret the absorption spectrum on the basis of the semiclassical simulation.

The simulation of the UV spectrum was done with 100 000 samplings. Figure 4 shows the total absorption cross section and the bands due to only the most intense transitions. As already noted, the lowest electronic transition, placed at 2.64 eV (470 nm), is due to the 1^1B_1 state. This state brings about a band fairly well separated from the next ones. In comparison with the experimental spectrum (Figure 4), which has a maximum $\sigma = 0.01$ Mbarn, the calculated oscillator strength is clearly incorrect by an order of magnitude. This confirms the difficulty of accurately calculating small transition dipole moments. The second broad band, placed between 3.8 and 5.5 eV (325−225 nm) with a maximum σ of 1.8 Mbarn, appears to be produced by more than one transition; in fact, we found that three states placed in this spectral region give almost the same absorption intensities, with the 1^1B_2 state (maximum of 1.4 Mbarn at 4.2 eV) giving the largest contribution to this band. In this assignment, we agree with Nickolaisen et al.[20] The other two transitions are due respectively to 2^1A_1 (maximum at 0.43 Mbarn and 4.4 eV) and 2^1A_2 (maximum at 0.17 Mbarn and 4.9 eV) states. The sum of these three peaks gives a band centered at 4.4 eV (280 nm) with a maximum σ of 1.9 Mbarn, very similar to the experimental result. The next observed band ranges from 5.5 to 8 eV. Here, we have two peaks, the first one with $\sigma = 13.4$ Mbarn at 7.2 eV (172 nm) and the second one, vibrationally structured, with average $\sigma \sim 15$ Mbarn around 7.7 eV (160 nm). Our simulation shows that several states contribute to this broad band: the 4^1A_1 and the 2^1B_1 states contribute to the long wavelength tail, but the first peak is dominated by the 3^1B_2 state with maximum $\sigma = 33.1$ Mbarn at 7.0 eV (178 nm). In the past, this peak has been attributed to the $^1B_1$[20] or $^1A_1$[39] state. The second peak is produced by a transition to the 4^1B_1 state (maximum at 13.2 Mbarn and 7.7 eV). The nature of the vibrational structure will be discussed below.

In Table 6, we summarize the analysis of the electronic configuration of the excited states at the equilibrium geometry. The valence molecular orbitals lying in the molecular plane are

labeled as n, σ, and σ^* according to their bonding properties (a_1 and b_2 irreps), while the perpendicular ones are labeled π, π_{nb}, and π^* (a_2 and b_1).

We remark that the two antibonding orbitals have different characters in view of the possibility of forming a Cl−Cl bond: the $\sigma^*_{a_1}$ could form a π_{Cl-Cl} in the case of symmetric dissociation of the Cl−O bonds, whereas $\sigma^*_{b_2}$ only produces a π_{Cl-Cl}^*. Even if a detailed analysis of the dissociation pathways is beyond the scope of this paper, we note that every excited state could bring about the dissociation of one or both Cl−O bonds, but only some of them could lead to the formation of molecular chlorine. The 4^1B_1 state, which produces the last peak of the simulated spectrum, clearly has a Rydberg character. As already proposed,[23] it originates from a transition to a Rydberg orbital of s character. Therefore, the vibrationally structured peak placed at 7.7 eV is probably due to a locally bound potential, parallel to that of the Cl_2O^+ ground state.

Conclusions

We have presented an ab initio study of the electronic structure and absorption spectra in two molecules of atmospheric interest, ClOOCl and Cl_2O. This investigation is more complete than previous work, in that we simulated the electronic spectra by computing semiclassical absorption cross sections. Moreover, for Cl_2O we extended the range of computed excited states with respect to previous calculations. As is well-known, the ab initio calculation of very small oscillator strengths easily leads to large relative errors: therefore, we cannot solve the uncertainties that affect the long-wavelength tail of the measured cross sections. However, the good general agreement with the experimental spectra allows us to assign all bands up to 5.5 eV for ClOOCl and 8.0 eV for Cl_2O. In particular, we can distinguish three regions in the ClOOCl spectrum: from 220 to 260 nm, one excites the 3^1B state; from 260 to 320 nm, the states are 4^1A, 2^1B, and 3^1A; with $\lambda > 320$ nm, the states are 1^1B and 2^1A. The nature of the excited states may influence the photochemistry; in other words, one may expect wavelength-dependent quantum yields. To investigate these aspects, we shall undertake simulations of the photodissociation dynamics based on more complete potential energy surfaces.

References and Notes

(1) Wayne, R. P.; Poulet, G.; Biggs, P.; Burrows, J. P.; Cox, R. A.; Crutzen, P. J.; Hayman, G. D.; Jenkin, M. E.; LeBras, G.; Moortgat, G. K.; Platt, U.; Schindler, R. N. *Atmos. Environ.* **1995**, *29*, 2675.

(2) De More, W. B.; Sander, S. P.; Golden, D. M.; Hampson, R. F.; Kurylo, M. J.; Howard, C. J.; Ravishankara, A. R.; Kolb, C. E.; Molina, M. J. Publication 97-4; Jet Propulsion Laboratory: Pasadena, CA, 1997.

(3) Sander, S. P.; Friedl, R. R.; De More, W. B.; Golden, D. M.; Krylo, M. J.; Hampson, R. F.; Huie, R. E.; Moortgat, G. K.; Ravishankara, A. R.;

Kolb, C. E.; Molina, M. J. Publication 00-3; Jet Propulsion Laboratory: Pasadena, CA, 2000.

(4) Toniolo, A.; Persico, M.; Pitea, D. *J. Chem. Phys.* **2000**, *112*, 2790.

(5) Lane, I. C.; Howie, H.; Orr-Ewing, A. J. *Phys. Chem. Chem. Phys.* **1999**, *1*, 3087.

(6) Howie, W. H.; Lane, I. C.; Newman, S. M.; Johnson, D. A.; Orr-Ewing, A. *J. Phys. Chem. Chem. Phys.* **1999**, *1*, 3079.

(7) Peterson, K. A.; Werner, H.-J. *J. Chem. Phys.* **1996**, *105*, 9823.

(8) Molina, L. T.; Molina, M. J. *J. Phys. Chem.* **1987**, *91*, 433.

(9) Cox, R. A.; Hayman, G. D. *Nature* **1988**, *332*, 796.

(10) Molina, M. J.; Colussi, A. J.; Schindler, R. N.; Tso, T.-L. *Chem. Phys. Lett.* **1990**, *173*, 310.

(11) Moore, T. A.; Okumura, M.; Seale, J. W.; Minton, T. K. *J. Phys. Chem. A* **1999**, *103*, 1691.

(12) Stanton, J. F.; Bartlett, R. J. *J. Chem. Phys.* **1993**, *98*, 9335.

(13) Permien, T.; Vogt, R.; Schindler, R. N. Mechanisms of Gas Phase-Liquid-Phase Chemical Transformations. In *Air Pollution Report #17*; Cox, R. A., Ed.; Environmental Research Program of the CEC: Brussels, 1988.

(14) De More, W. B.; Tschuikow-Roux, E. *J. Phys. Chem.* **1990**, *94*, 5856.

(15) Burkholder, J. B.; Orlando, J. J.; Howard, C. J. *J. Phys. Chem.* **1990**, *94*, 687.

(16) Huder, K. J.; De More, W. B. *J. Phys. Chem.* **1995**, *99*, 3905.

(17) Donsig, H. A.; Herridge, D.; Vickerman, J. C. *J. Phys. Chem. A* **1998**, *102*, 2302.

(18) Banham, S. F.; Horn, A. B.; Koch, T. G.; Sodeau, J. R. *Faraday Discuss.* **1995**, *100*, 321.

(19) Tanaka, Y.; Kawasaki, M.; Matsumi, Y.; Fujiwara, H.; Ishiwata, T.; Rogers, L. J.; Dixon, R. N.; Ashfold, M. N. R. *J. Chem. Phys.* **1998**, *109*, 1315.

(20) Nickolaisen, S. L.; Miller, C. E.; Sander, S. P.; Hand, M. R.; Williams, S. P.; Francisco, J. S. *J. Chem. Phys.* **1996**, *104*, 2857.

(21) Nelson, C. M.; Moore, T. A.; Okumura, M.; Minton, T. K. *J. Chem. Phys.* **1994**, *100*, 8055.

(22) Knauth, H. D.; Alberti, H.; Clausen, H. *J. Phys. Chem.* **1979**, *83*, 1604.

(23) Motte-Tollet, F.; Ska, M.-P.; Marston, G. M.; Walker, I. C.; Siggel, M. R. F.; Gingell, J. M.; Kaminski, L.; Brown, K.; Mason, N. J. *Chem. Phys. Lett.* **1997**, *275*, 298.

(24) Schmidt, M. W.; Baldridge, K. K.; Boatz, J. A.; Elbert, S. T.; Gordon, M. S.; Jensen, J. H.; Koseki, S.; Matsunaga, N.; Nguyen, K. A.; Su, S. J.; Windus, T. L.; Dupuis, M.; Montgomery, J. A. *J. Comput. Chem.* **1993**, *14*, 1347.

(25) Schafer, A.; Horn, H.; Ahlrics, R. *J. Chem. Phys.* **1992**, *97*, 2571.

(26) Dunning, T. H., Jr. *J. Chem. Phys.* **1989**, *90*, 1007.

(27) Woon, D. E.; Dunning, T. H., Jr. *J. Chem. Phys.* **1993**, *98*, 1358.

(28) Andersson, K.; Blomberg, M. R. A.; Fülscher, M. P.; Karlström, G.; Lindh, R.; Malmqvist, P. Å.; Neogrády, P.; Olsen, J.; Roos, B. O.; Sadlej, A. J.; Schütz, M.; Seijo, L.; Serrano-Andrés, L.; Siegbahn, P. E. M.; Widmark, P. O. *MOLCAS*, Version 3.0; Lund University: Sweden, 1997.

(29) Cimiraglia, R. J. *Chem. Phys.* **1985**, *83*, 1746.

(30) Angeli, C.; Cimiraglia, R.; Persico, M.; Toniolo, A. *Theor. Chem. Acc.* **1997**, *98*, 57.

(31) Cimiraglia, R.; Malrieu, J.-P.; Persico, M.; Spiegelmann, F. *J. Phys. B* **1985**, *18*, 3073.

(32) Dunning, T. H., Jr.; Hay, J. P. In *Modern Theoretical Chemistry*; Schaefer, H. F., III, Ed.; Plenum: New York, 1977; Vol. 3, Chapter 1.

(33) Weide, K.; Schinke, R. *J. Chem. Phys.* **1989**, *90*, 7150.

(34) Jacobs, J.; Kronberg, M.; Müller, H. S. P.; Willner, H. *J. Am. Chem. Soc.* **1994**, *116*, 1106.

(35) Birk, M.; Friedl, M. M.; Cohen, E. A.; Pickett, H. M.; Sander, S. P. *J. Chem. Phys.* **1989**, *91*, 6588.

(36) Nakata, M.; Sugic, M.; Takeo, H.; Matsumura, C.; Fukuyama, T.; Kuchitsu, K. *J. Mol. Spectrosc.* **1981**, *86*, 241.

(37) Shimanouchi, T. In *Tables of Molecular Vibrational Frequencies*; US GPO: Washington, DC, 1972.

(38) Del Bene, J. E.; Watts, J. D.; Bartlett, R. J. *Chem. Phys. Lett.* **1995**, *246*, 541.

(39) Kuwata, K.; Goddard, W. A.; Okomura M. Personal communication, referenced in ref 21.